Supporting Information

Red Blood Cells-Derived Iron Self–Doped 3D Porous Carbon Networks for Efficient Oxygen Reduction

Zicong Zhang , Xiangli Ru *, Xiaoli Yang , Zhengyu Bai *, Lin Yang *

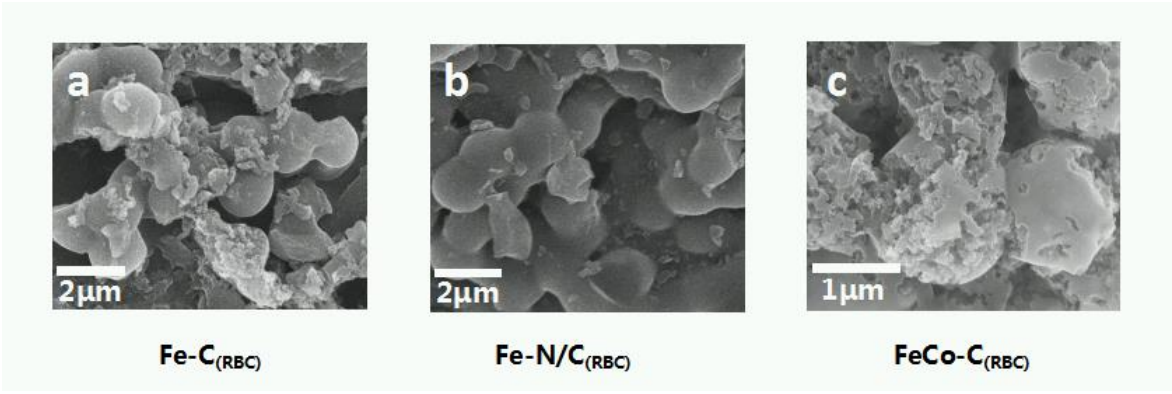

Figure S1. SEM images of Fe-$C_{(RBC)}$ (a), Fe-N/$C_{(RBC)}$ (b), FeCo-$C_{(RBC)}$(c).

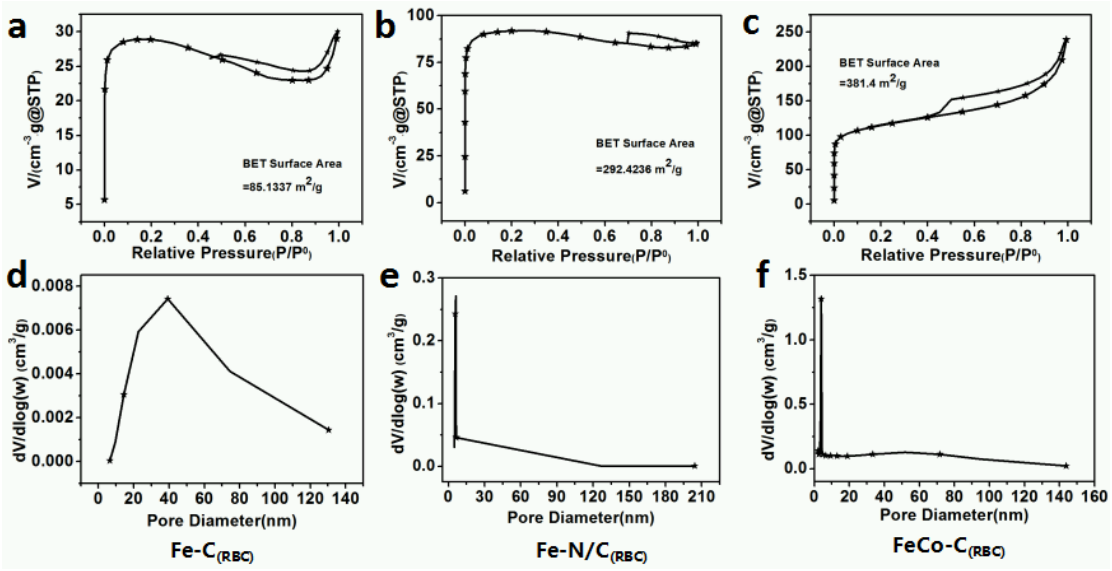

Figure S2. N_2 adsorption-desorption isotherms of Fe-$C_{(RBC)}$, Fe-N/$C_{(RBC)}$ and FeCo-$C_{(RBC)}$ (a-c), pore-size distributions of Fe-$C_{(RBC)}$, Fe-N/$C_{(RBC)}$ and FeCo-$C_{(RBC)}$ (d-f).

Table S1. Atomic content of C 1s, Fe 2p, N 1s, O 1s and Co 2p in Fe-$C_{(RBC)}$, Fe-N/$C_{(RBC)}$, FeCo-$C_{(RBC)}$ and FeCo-N/$C_{(RBC)}$ from XPS data.

	C1s at.%	Fe2p at.%	N1s at.%	O1s at.%	Co2p at.%
Fe-$C_{(RBC)}$	**89.91**	**0.59**	**4.48**	**5.02**	**-**
Fe-N/$C_{(RBC)}$	**88.12**	**0.57**	**5.42**	**5.89**	**-**
FeCo-$C_{(RBC)}$	**83.90**	**0.56**	**4.61**	**9.96**	**0.97**
FeCo-N/$C_{(RBC)}$	**83.13**	**0.54**	**5.36**	**10.01**	**0.96**

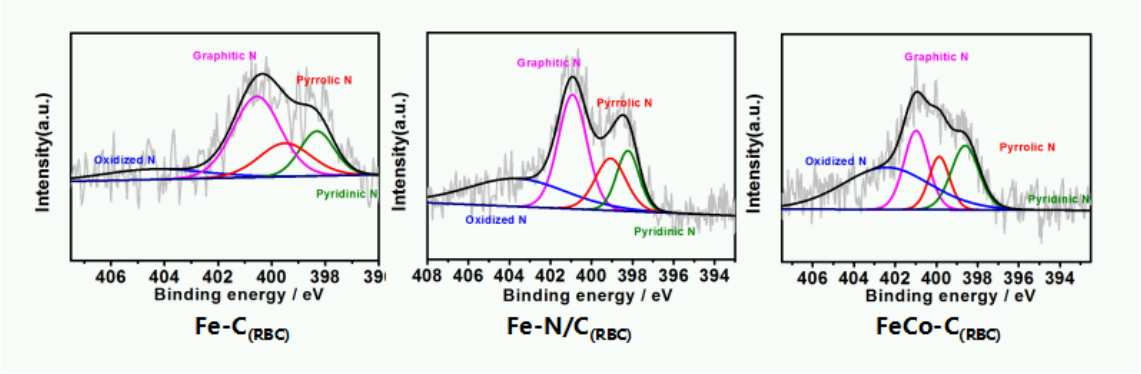

Figure S3. High-resolution N1s XPS spectrum of Fe-$C_{(RBC)}$,Fe-N/$C_{(RBC)}$ and FeCo-$C_{(RBC)}$.

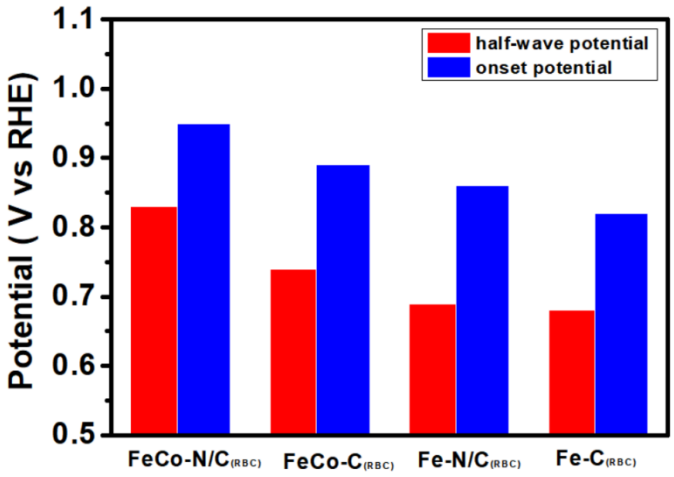

Figure S4. The histogram for onset potential and half wave potential of Fe-$C_{(RBC)}$, Fe-N/$C_{(RBC)}$, FeCo-$C_{(RBC)}$ and FeCo-N/$C_{(RBC)}$ in 0.1 M KOH solution.

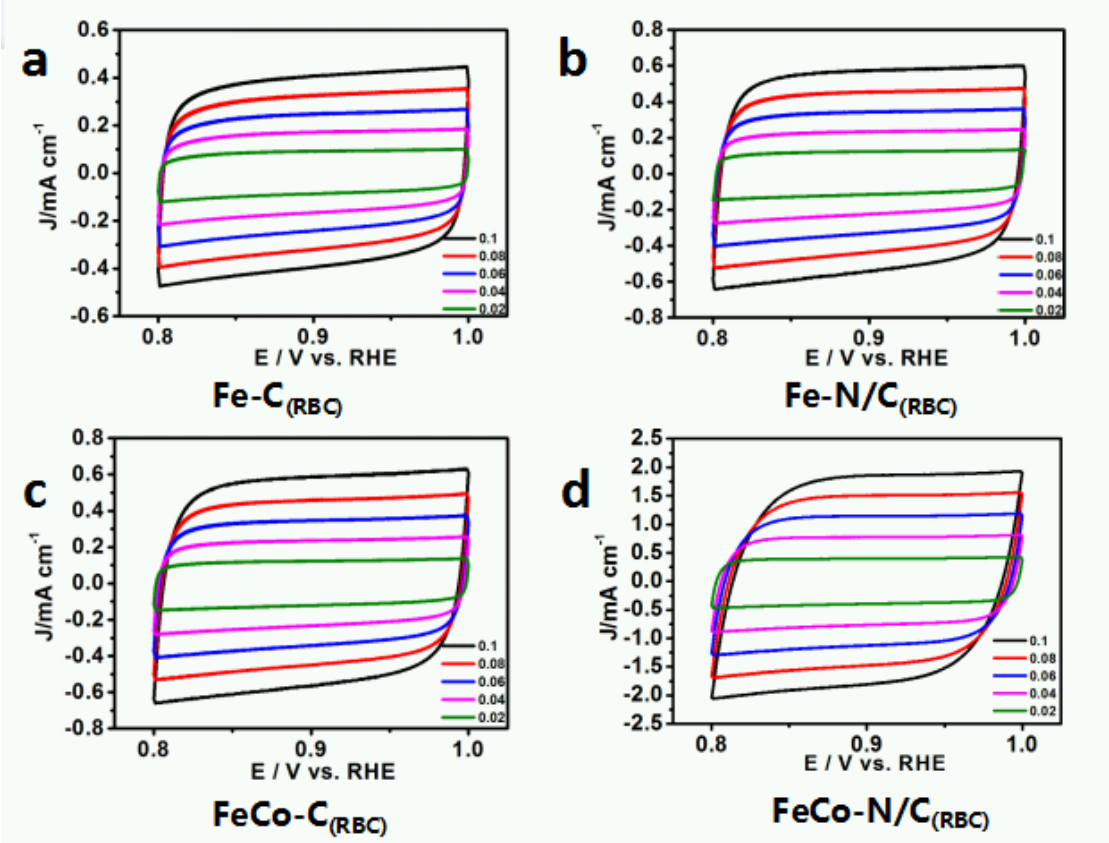

Figure S5. Cyclic voltammograms in the region without faradaic processes with different scan rates of Fe-$C_{(RBC)}$(a), Fe-N/$C_{(RBC)}$(b), FeCo-$C_{(RBC)}$(c) and FeCo-N/$C_{(RBC)}$(d).

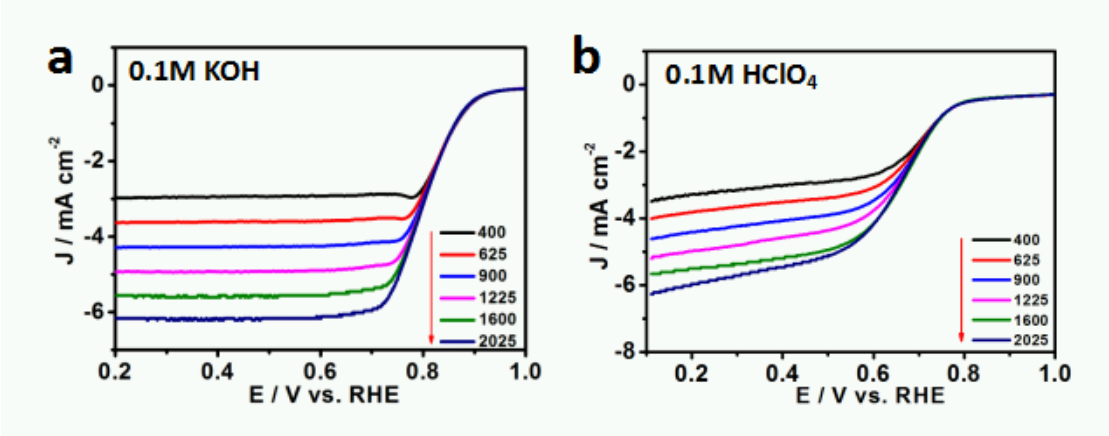

Figure S6. LSV curves of FeCo-N/$C_{(RBC)}$ at different rotation rate in O_2 saturated 0.1 M KOH solution(a) and 0.1M $HClO_4$ solution(b).

Table S2. The ORR activity data in 0.1 M KOH solution for FeCo-N/$C_{(RBC)}$ and other catalysts from previous reports.

Pt-free or Pt catalysts modified electrodes	Biomass Source	E_{ORR} / V	E_{hw} / V	j / mA cm^{-2}	References
20% Pt/C/GCE	-	0.96	0.87	5.5	
BP350C1000/GCE	Red blood cells	0.90	0.78	1.3	[1]
N-CNT(800)/GCE	Red blood cells	0.91	0.70	3.4	[2]
FeNC-900/GCE	Red blood cells	0.96	0.85	5.6	[3]
PBC/900/M/GCE	Red blood cells	1.01	0.86	5.2	[4]
Co16%-NCNT-T900/GCE	Chitosan	-	0.84	5.0	[5]
Fe-NP-SP/GCE	Woody biomass	1.07	0.87	-	[6]
D-PC-1(900)/GCE	Seaweed	1.01	0.83	5.4	[7]
CoOP@bio-C/GCE	Peanut shells	0.91	0.81	5.7	[8]
GPNCS/GCE	Privet fruit	-	0.81	-	[9]
NCF900/GCE	Catkins	0.82	0.66	3.7	[10]
AC_1/GCE	Agave sisalana	0.84	-	3.12	[11]
PN/CB/GCE	Pine needles	0.86	0.78	-	[12]
AOB700/GCE	Onion peels	0.82	-	2.35	[13]
N-P-Fe-C/GCE	Corn silk	0.95	0.85	-	[14]
$NPAC_{Co}$/GCE	Pomelo peels	0.87	0.78	-	[15]
AC-F-U-P/GCE	Coconut shells	0.96	0.77	-	[16]
FeCo-N/$C_{(RBC)}$/GCE	Red blood cells	0.95	0.83	5.5	This work

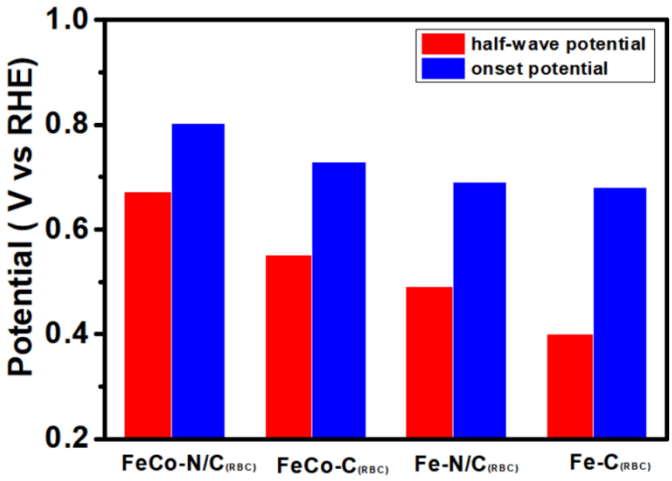

Figure S7. The histogram for onset potential and half wave potential of Fe-$C_{(RBC)}$, Fe-$N/C_{(RBC)}$, FeCo-$C_{(RBC)}$ and FeCo-$N/C_{(RBC)}$ in 0.1 M $HClO_4$ solution.

References

1. Guo, C.-Z.; Chen, C.-G.; Luo, Z.-L. A novel nitrogen-containing electrocatalyst for oxygen reduction reaction from blood protein pyrolysis. *J. Power Sources* **2014**, *245*, 841–845. https://doi.org/10.1016/j.jpowsour.2013.07.037.
2. Zheng, J.; Guo, C.; Chen, C.; Fan, M.; Gong, J.; Zhang, Y.; Zhao, T.; Sun, Y.; Xu, X.; Li, M.; et al. High content of pyridinic- and pyrrolic-nitrogen-modified carbon nanotubes derived from blood biomass for the electrocatalysis of oxygen reduction reaction in alkaline medium. *Electrochim. Acta* **2015**, *168*, 386–393. https://doi.org/10.1016/j.electacta.2015.03.173.
3. Jiang, W.-J.; Hu, W.-L.; Zhang, Q.-H.; Zhao, T.-T.; Luo, H.; Zhang, X.; Gu, L.; Hu, J.-S.; Wan, L.-J. From biological enzyme to single atomic Fe–N–C electrocatalyst for efficient oxygen reduction. *Chem. Commun.* **2018**, *54*, 1307–1310. https://doi.org/10.1039/c7cc08149a.
4. Lee, J.; Kim, H.S.; Jang, J.-H.; Lee, E.-H.; Jeong, H.-W.; Lee, K.-S.; Kim, P.; Yoo, S.J. Atomic-Scale Engineered Fe Single-Atom Electrocatalyst Based on Waste Pig Blood for High-Performance AEMFCs. *ACS Sustain. Chem. Eng.* **2021**, *9*, 7863–7872. https://doi.org/10.1021/acssuschemeng.1c01590.
5. Zhang, Y.; Lu, L.; Zhang, S.; Lv, Z.; Yang, D.; Liu, J.; Chen, Y.; Tian, X.; Jin, H.; Song, W. Biomass chitosan derived cobalt/nitrogen doped carbon nanotubes for the electrocatalytic oxygen reduction reaction. *J. Mater. Chem. A* **2018**, *6*, 5740–5745. https://doi.org/10.1039/c7ta11258k.
6. Li, Y.; Liu, D.; Gan, J.; Duan, X.; Zang, K.; Rønning, M.; Song, L.; Luo, J.; Chen, D. Sustainable and Atomically Dispersed Iron Electrocatalysts Derived from Nitrogen- and Phosphorus-Modified Woody Biomass for Efficient Oxygen Reduction. *Adv. Mater. Interfaces* **2018**, *6*, 6. https://doi.org/10.1002/admi.201801623.
7. Hao, Y.; Zhang, X.; Yang, Q.; Chen, K.; Guo, J.; Zhou, D.; Feng, L.; Slanina, Z. Highly porous defective carbons derived from seaweed biomass as efficient electrocatalysts for oxygen reduction in both alkaline and acidic media. *Carbon* **2018**, *137*, 93–103. https://doi.org/10.1016/j.carbon.2018.05.007.
8. Wu, Y.; Chen, Y.; Wang, H.; Wang, C.; Wang, A.; Zhao, S.; Li, X.; Sun, D.; Jiang, J. Efficient ORR electrocatalytic activity of peanut shell-based graphitic carbon microstructures. *J. Mater. Chem. A* **2018**, *6*, 12018–12028. https://doi.org/10.1039/c8ta02839g.
9. Liu, Y.; Sun, K.; Cui, X.; Li, B., Jiang, J. Defect-Rich, Graphenelike Carbon Sheets Derived from Biomass as Efficient Elec-trocatalysts for Rechargeable Zinc–Air Batteries. *ACS Sustain. Chem. Eng.* **2020**, *8*, 2981–2989.

10. Liu, A.; Ma, M.; Zhang, X.; Ming, J.; Jiang, L.; Li, Y.; Zhang, Y.; Liu, S. A biomass derived nitrogen doped carbon fibers as efficient catalysts for the oxygen reduction reaction. *J. Electroanal. Chem.* **2018**, *824*, 60–66. https://doi.org/10.1016/j.jelechem.2018.07.039.
11. Fernandes, D.M.; Mestre, A.S.; Martins, A.; Nunes, N.; Carvalho, A.P.; Freire, C. Biomass-derived nanoporous carbons as electrocatalysts for oxygen reduction reaction. *Catal. Today* **2020**, *357*, 269–278. https://doi.org/10.1016/j.cattod.2019.02.048.
12. Gao, J.; Chu, X.; He, C.; Yin, Z.; Lu, H.; Li, X.; Feng, J.; Tan, X. Biomass-derived carbon for ORR: Pine needles as a single source for efficient carbon electrocatalyst. *J. Appl. Electrochem.* **2020**, *50*, 1257–1267. https://doi.org/10.1007/s10800-020-01483-4.
13. Alonso-Lemus, I.L.; Escobar-Morales, B.; Lardizabal-Gutierrez, D.; de la Torre-Saenz, L.; Quintana-Owen, P.; Rodriguez-Varela, F. Short communication: Onion skin waste-derived biocarbon as alternative non-noble metal electrocatalyst towards ORR in alkaline media. *Int. J. Hydrogen Energy* **2018**, *44*, 12409–12414. https://doi.org/10.1016/j.ijhydene.2018.10.050.
14. Wan, W.; Wang, Q.; Zhang, L.; Liang, H.-W.; Chen, P.; Yu, S.-H. N-, P- and Fe-tridoped nanoporous carbon derived from plant biomass: An excellent oxygen reduction electrocatalyst for zinc–air batteries. *J. Mater. Chem. A* **2016**, *4*, 8602–8609. https://doi.org/10.1039/c6ta02150f.
15. Zhang, M.; Jin, X.; Wang, L.; Sun, M.; Tang, Y.; Chen, Y.; Sun, Y.; Yang, X.; Wan, P. Improving biomass-derived carbon by activation with nitrogen and cobalt for supercapacitors and oxygen reduction reaction. *Appl. Surf. Sci.* **2017**, *411*, 251–260. https://doi.org/10.1016/j.apsusc.2017.03.097.
16. Borghei, M.; Laocharoen, N.; Kibena-Põldsepp, E.; Johansson, L.-S.; Campbell, J.; Kauppinen, E.; Tammeveski, K.; Rojas, O.J. Porous N,P-doped carbon from coconut shells with high electrocatalytic activity for oxygen reduction: Alternative to Pt-C for alkaline fuel cells. *Appl. Catal. B Environ.* **2017**, *204*, 394–402. https://doi.org/10.1016/j.apcatb.2016.11.029.